Analysis of the Dynamic Forces of 3D Printer with 4 Degrees of Freedom

Sajjad Pakzad *
Faculty of Design,
Tabriz Islamic Art University, Iran
E-mail: s.pakzad@tabriziau.ac.ir
*Corresponding author

Ebrahim Imani
Faculty of Design,
Tabriz Islamic Art University, Iran
Department of PDTA, Sapienza University of Rome, Rome, Italy
E-mail: e.imani@tabriziau.ac.ir

Abstract: The use of parallel mechanisms in the structure of 3D printers are developing. Parallel mechanisms have excellent capabilities in terms of accuracy, stiffness and high load-bearing capacity. This article studies a 3D printer with four degrees of freedom that has three degrees of linear freedom and one degree of rotational freedom. The advantages of this printer are greater than conventional Cartesian printers, including higher print speed and stiffness, and there are also higher degrees of freedom for manoeuvrability. In this paper, the Newton-Euler analytical method is used to analyse the inverse dynamics and identify the driving forces required by the 3D nozzle motion. By coding the inverse dynamic equations in the MATLAB software environment, the driving forces diagrams are extracted based on the printer's nozzle motion. To validate the inverse dynamics relationships, simulations with the Simmechanic model of MATLAB software have been performed. Through changing the speed of movement of the printer nozzle and also change of the velocity and acceleration of drives, the forces required for the drive also change. The effect of changes in print speed of a specific geometry on the driving forces is also studied. As well as, choosing the optimum print speed with regard to the motor driver power and the dynamics of the forces applied to the drivers and the less print time are the most important factors that are discussed in this article.

Biographical notes: Sajjad Pakzad received his PhD in Mechanical Engineering from University of Tabriz, Tabriz, Iran, in 2018. Dr. Pakzad is currently assistant professor in the Faculty of Design in Tabriz Islamic Art University, Tabriz, Iran. His research interests include Industrial Design, Parallel Mechanism and Robotics. **Ebrahim Imani** is currently a PhD student at the Product Design at the Department of PDTA (Planning, Design, Architecture Technology) in the Sapienza University of Rome, Rome, Italy. His research interests include Design Process Management, DFMA, and Design in Industry 4.0.

1 INTRODUCTION

With the advancement of industries, especially the aerospace and military industries, the use of complex components with high precision was required which traditional machinery were not affordable. Parallel mechanisms are widely used in any engineering sciences and industrial contexts, such as machinery, metrology, flight simulator, earthquake simulator, medical equipment and more are included. In general, these mechanisms have two main bodies that are coupled through multiple links which operate in parallel [1]. There has been a lot of research on parallel robots in recent years.

One of the developments currently underway in industrial production especially in the manufacturing sector, is the use of parallel mechanisms in 3D printing. Parallel robots with six degrees of freedom, generally suffer from the small workspace, complicated mechanical design, control and difficult movement due to their complex kinematic analysis. To overcome these shortcomings, new structures are used for parallel robots with less than six degrees of freedom. On the other hand, in many industrial cases, there is a need for equipment to provide more than three degrees of freedom arranged in parallel and based on a simpler layout than six degrees of freedom [2].

Dynamic modelling of a parallel mechanism in terms of its ability to control of motion, especially when precise positioning and proper dynamic performance of the mechanism with load on it is desired, is of particular importance and is the first step in vibrational analysis and mechanism control, that is why it has been the subject of various studies. Unlike open loop series mechanisms, dynamic modelling of parallel mechanisms due to kinematic constraints and closed loop chains has inherent computational complexity [3], [4].

Numerous methods, based on classical mechanics, have been proposed by researchers for the dynamic analysis of parallel mechanisms. Geng et al. [5], Lebret et al. [6] and Pang and Shahinpoor [7] proposed the Euler-Lagrange method for solving Stewart platform equations of motion; this method also has been used in references [8-9]. The use of Newton-Euler method in solving the dynamic equations of the intended mechanism, because of its independence of calculating most of the partial derivatives and limited volume of numerical computation, and also, the ability to derive closed-form dynamic equations, has a particular advantage over the Euler-Lagrange method [5]. Do & Yang [10], Reboulet and his colleague [11], Ji [12], Harib [13], Dasgupta and his colleague [14-16], Riebe and his colleague [17], Guo and Li [18], Khalil and Ibrahim [19], Wang et al. [20] and Mahmoodi et al. [21], have used the Newton-Euler method to solve the dynamical equations of the mechanism using simplification assumptions. The kinematics and dynamics of parallel mechanisms have also been studied by researchers with using other foundations of classical mechanics which can be noted employing virtual work [22-25], the Lagrange formula [5], [26-29] and the Hamiltonian principle [30]. Kebria et al. Have presented a CAD model of the Gentry Tao robot and a Simmechanic model in the environment of MATLAB. Finally, the simulation of the Simmechanic model that has been shown can be used for analysing, controlling simulation, optimizing and designing the robot [31].

As presented in the paper research background; the dynamics of different mechanisms have been analyzed by researchers in various ways such as Newton-Euler, Lagrange, Virtual Work and Hamilton. Therefore, due to the use of Newton-Euler method in solving dynamic equations, owing to the need to calculate many partial derivatives and the limited amount of numerical computations needed and also the ability to derive closed-loop dynamic equations, it has a particular advantage over other methods. In the present study, the Newton-Euler analytical method is used to analyse the dynamic forces of a 3D printer with 4 degrees of freedom proposed also in many studies that using the Newton-Euler method have ignored and simplified joint friction and links mass.

However, in the present study, the frictional force of the sliding joints and the mass of the links are also taken into the calculations. Dynamic analysis, along with kinematic analysis, brings us closer to reality in our understanding of the motion mechanism. In the Inverse Dynamics Method, the identification of the driving forces required by the type of nozzle movement is considered. This analysis plays a key role in the optimal control of the proposed 4 degrees of freedom mechanism. Inverse dynamic equations for the proposed printer have been extracted and applied by the program and written in the MATLAB software environment and applied by the designed mechanism.

2 INTRODUCING 3D PRINTERS WITH 4 DOF

In this paper, a 3D printer with the four degrees of freedom shown in "Fig. 1" is studied. The present robot which uses a parallel mechanism, has four pods that are connected to a platform which is a kind of parallel mechanisms with fixed pods length, that fixed pods length makes the mechanism more rigid. The parallel mechanism provides 4 degrees of freedom for the robot, including movement in the x, y and z axes and the rotation around the x axis. The presence of a fourth degree of freedom (rotational motion) increases the manoeuvrability and efficiency of the mechanism compared to the three degrees of freedom.
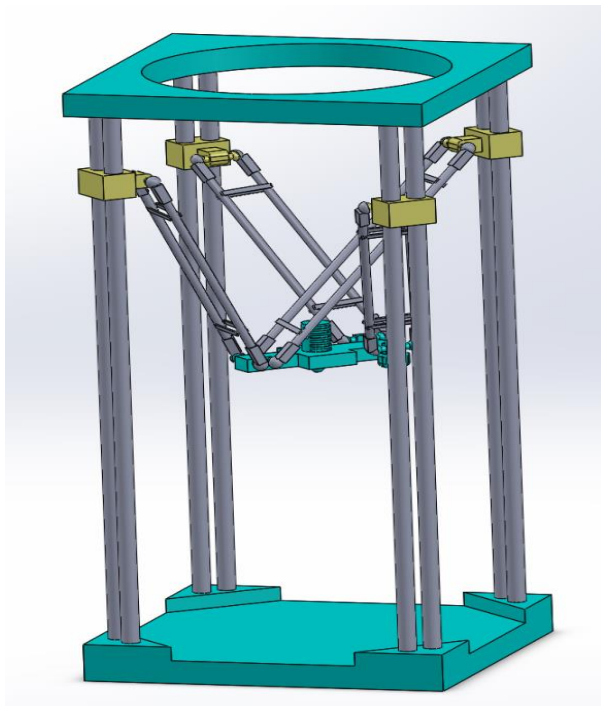
Fig. 1 3D Printer with 4 Degrees of Freedom.

3 INVERSE DYNAMIC ANALYSIS

As shown in "Fig. 2", Eulerian equations [32] of the parallelogram links around the n axis (the parallelogram direction of rotation) for each link are as follows:

$$\begin{pmatrix} \mathbf{U}_1\mathbf{M}_1 \times \mathbf{F}_{ru} + \kappa \times \mathbf{F}_{inl} + \mathbf{U}_1\mathbf{N}_1 \times \mathbf{F}_{rd} \\ + \mathbf{l} \times \mathbf{F}_{D1} + \mathbf{M}_{inl} + \mathbf{M}_{ru1} + \mathbf{M}_{rd1} \end{pmatrix} \cdot \mathbf{n} = 0 \qquad (1)$$

$$\begin{pmatrix} \mathbf{U}_2\mathbf{M}_2 \times (-\mathbf{F}_{ru}) + \kappa \times \mathbf{F}_{inl} + \mathbf{U}_2\mathbf{N}_2 \times (-\mathbf{F}_{rd}) \\ + \mathbf{l} \times \mathbf{F}_{D2} + \mathbf{M}_{inl} + \mathbf{M}_{ru2} + \mathbf{M}_{rd2} \end{pmatrix} \cdot \mathbf{n} = 0 \qquad (2)$$

Where, the $\mathbf{F}_{ru}$, $\mathbf{F}_{rd}$, $\mathbf{M}_{ru}$ and $\mathbf{M}_{rd}$ are forces and torques inflicted on the links by the beams between the parallelograms, $\mathbf{F}_D$ is the forces exerted on the links by the moving platform, $\mathbf{F}_{inl}$ and $\mathbf{M}_{inl}$ are the forces and moments of inertia at the centre of mass of the link.
By summing "Eqs. (1) and (2)" and taking into account that the beams are connected to the links by the revolute joint $\mathbf{M}_{ru} \cdot \mathbf{n} = \mathbf{M}_{rd} \cdot \mathbf{n} = 0$ and mathematical relationships, we have:

$$(\mathbf{l} \times \mathbf{n}) \cdot (\mathbf{F}_{D1} + \mathbf{F}_{D2}) = 2(\kappa \times \mathbf{F}_{inl} + \mathbf{M}_{inl}) \cdot \mathbf{n} \qquad (3)$$
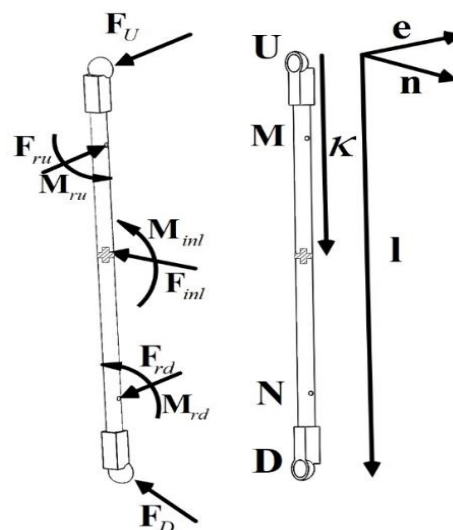
Fig. 2 The free diagram of the link.

Moreover, the Eulerian equation is applied to the parallelograms around the axis **e** is in the order below:

$$(2\kappa \times \mathbf{F}_{inl} + \mathbf{l} \times \mathbf{F}_{D1} + \mathbf{l} \times \mathbf{F}_{D2} + 2\mathbf{M}_{inl}) \cdot \mathbf{e} = 0 \qquad (4)$$

By rewriting the above equation and the mathematical relations we have:

$$(\mathbf{l} \times \mathbf{e}) \cdot (\mathbf{F}_{D1} + \mathbf{F}_{D2}) = 2(\kappa \times \mathbf{F}_{inl} + \mathbf{M}_{inl}) \cdot \mathbf{e} \qquad (5)$$

By writing "Eqs. (3) and (5)" for all the links, the following equations can be obtained:

$$\begin{bmatrix} \mathbf{l} \times \mathbf{n} \\ \mathbf{l} \times \mathbf{e} \end{bmatrix} [\mathbf{F}_{D1} + \mathbf{F}_{D2}] = \begin{bmatrix} 2(\kappa \times \mathbf{F}_{inl} + \mathbf{M}_{inl}) \cdot \mathbf{n} \\ 2(\kappa \times \mathbf{F}_{inl} + \mathbf{M}_{inl}) \cdot \mathbf{e} \end{bmatrix} \qquad (6)$$

Figure 3 shows the free diagram of the forces and torques applied to the joint. The Newton relation for the joint is written as follows:

$$\mathbf{F}_P = \mathbf{F}_{D1} + \mathbf{F}_{D2} - \mathbf{F}_{inJ} \qquad (7)$$

The $\mathbf{F}_P$ is the force exerted by the moving platform to the joint and the $\mathbf{F}_{inJ}$ is the inertia force applied to the centre of mass of the joint. Referring to "Fig. 4", the Eulerian relation of the moving platform around the axis passing through R_1 and R_3 is written as follows:

$$(\mathbf{r}_P \times \mathbf{F}_{inP} + \mathbf{M}_{inP} - \mathbf{M}_{Pi} - \mathbf{r}_i \times (\mathbf{F}_{D1,i} + \mathbf{F}_{D2,i})) \cdot \mathbf{i} = 0 \qquad (8)$$

Where $\mathbf{M}_P$ represents the torque of the joint to the moving platform, $\mathbf{F}_{inP}$ and $\mathbf{M}_{inP}$ are inertial forces and

moments acting on the centre of mass of moving platform. Given the existence of the revolute joint and the assumption of zero friction for it, $\mathbf{M}_P$ does not have any components around $\mathbf{i}$ and is written using the mathematical equations of "Eq. (8)":

$$[\mathbf{i} \times \mathbf{r}_{i=2,4}][\mathbf{F}_{D1} + \mathbf{F}_{D2}] = [(\mathbf{r}_P \times \mathbf{F}_{inP} + \mathbf{M}_{inP}) \cdot \mathbf{i}] \tag{9}$$
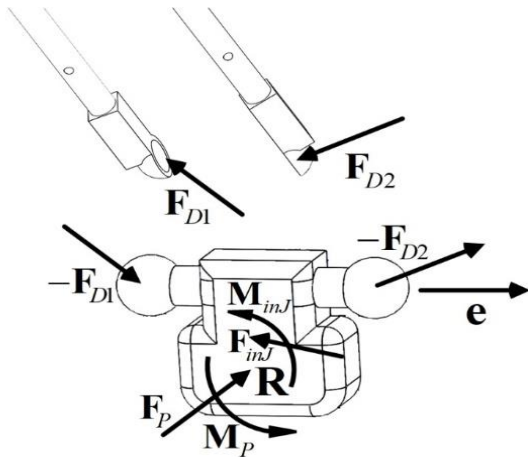
Fig. 3   The free diagram of the joint.
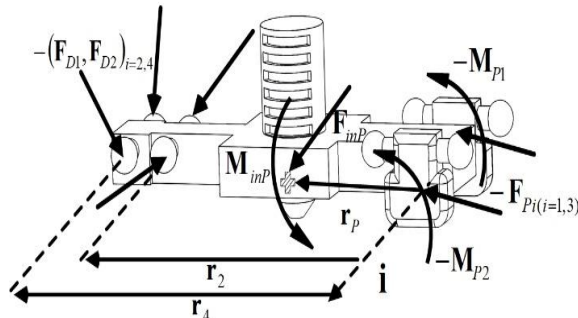
Fig. 4   The free diagram of the moving platform.

In addition by writing Newtonian relation to the moving platform, we have:

$$(\mathbf{F}_{D1} + \mathbf{F}_{D2})_{i=2,4} + \mathbf{F}_{Pi(i=1,3)} = \mathbf{F}_{inP} \tag{10}$$

By putting "Eq. (7) into Eq. (10)" we have:

$$[\mathbf{I}][\mathbf{F}_{D1} + \mathbf{F}_{D2}] = [\mathbf{F}_{inP} + \mathbf{F}_{inJ,1} + \mathbf{F}_{inJ,3}] \tag{11}$$

With the coupling matrices (6), (9) and (11) we have:

$$\begin{bmatrix} \mathbf{I} \\ \mathbf{i} \times \mathbf{r}_{i=2,4} \\ \mathbf{l} \times \mathbf{n} \\ \mathbf{l} \times \mathbf{e} \end{bmatrix} [\mathbf{F}_{D1} + \mathbf{F}_{D2}] = \begin{bmatrix} \mathbf{F}_{inP} + \mathbf{F}_{inJ,1} + \mathbf{F}_{inJ,3} \\ (\mathbf{r}_P \times \mathbf{F}_{inP} + \mathbf{M}_{inP}) \cdot \mathbf{i} \\ 2(\kappa \times \mathbf{F}_{inl} + \mathbf{M}_{inl}) \cdot \mathbf{n} \\ 2(\kappa \times \mathbf{F}_{inl} + \mathbf{M}_{inl}) \cdot \mathbf{e} \end{bmatrix} \tag{12}$$

Now consider the free diagram of "Fig. 5" and writing the Newtonian relation of the forces on the slider and the parallelogram mechanism, the following equation is obtained:

$$\mathbf{F}_S + (\mathbf{F}_{D1} + \mathbf{F}_{D2}) + \mathbf{F}_{inS} + 2\mathbf{F}_{inl} = 0 \tag{13}$$

Where, $\mathbf{F}_S$ is the force applied by the rail to slider and $\mathbf{F}_{inS}$ is slider inertial force.

Since the driving force is a component of force $\mathbf{F}_S$ in direction of $\mathbf{k}$, so the driving force $\mathbf{i}_{th}$ is obtained as follows:

$$f_S = \mathbf{F}_S \cdot \mathbf{k} \tag{14}$$

Thus, by integrating "Eqs. (12) and (13)" into "Eq. (14)", the driving forces are obtained:

$$f_S = -[\mathbf{k}] \left(\begin{bmatrix} \mathbf{F}_{inP} + \mathbf{F}_{inJ,1} + \mathbf{F}_{inJ,3} \\ (\mathbf{r}_P \times \mathbf{F}_{inP} + \mathbf{M}_{inP}) \cdot \mathbf{i} \\ 2(\kappa \times \mathbf{F}_{inl} + \mathbf{M}_{inl}) \cdot \mathbf{n} \\ 2(\kappa \times \mathbf{F}_{inl} + \mathbf{M}_{inl}) \cdot \mathbf{e} \end{bmatrix} \begin{bmatrix} \mathbf{I} \\ \mathbf{i} \times \mathbf{r}_{i=2,4} \\ \mathbf{l} \times \mathbf{n} \\ \mathbf{l} \times \mathbf{e} \end{bmatrix}^{-1} + [\mathbf{F}_{inS} + 2\mathbf{F}_{inl}] \right) \tag{15}$$

In this section, depending on the direction of movement of the moving platform, the driving forces can be obtained. Using this relation, the inverse dynamics goal, which is the calculation of the driving forces with respect to the movement of the moving platform, is achieved.
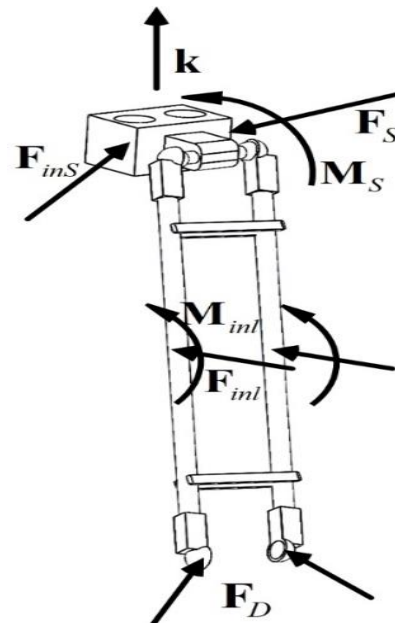
Fig. 5   The free diagram of the slider and pod.

4   MODEL VERIFYING

In this section, simulations are performed to validate the force relations of the mechanism. For this purpose, an example of a path for moving platform is considered, and the driving forces obtained from the theoretical method of solving the equations in MATLAB software are compared with the Simmechanic model of MATLAB software. In the validation process the results of the mathematical model obtained in the previous section are compared with the corresponding results of the Simmechanic model.

4.1. Simmechanic Model

MATLAB's Simmechanic Module provides a simulation environment for mechanical systems such as robots, car suspensions, mechanical equipment, structures and many other mechanisms. In this environment a mechanical system can be introduced by using body, joints, constraints, force and torque elements, coordinate systems and sensors. The Simmechanic for the created model, creates and solves the equations of motion. The mechanism assembly model can be entered into the Simmechanic environment with all dimensional, inertial, joints and constraints characteristics and can be viewed in 3D.

The main block of the Simmechanic model is shown in "Fig. 6". The model of the Simmechanic shown is comprised of six main sections as: 1- input, 2- Base, 3- Sliders, 4- Links, 5- Moving Platform, 6- Driving Forces Output.
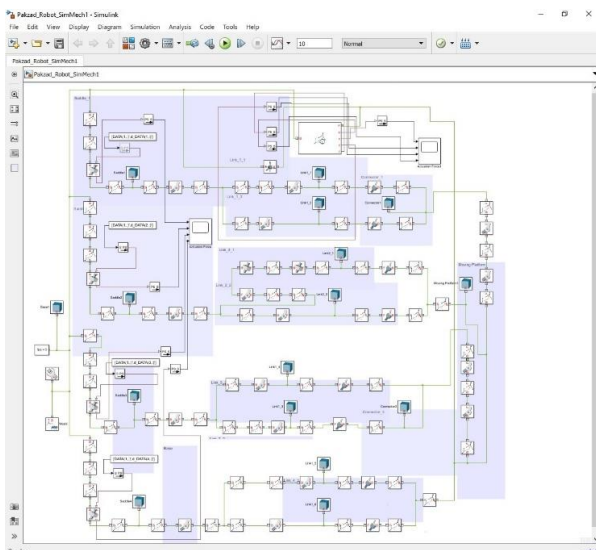
Fig. 6   The main block of the Simmechanic model of the studied mechanism.

4.1.1. Input

Simmechanic inputs are obtained from inverse kinematic analysis and entered into the model. This input is applied to the sliders as movement information, and the moving platform traverses its specified motion mechanism.

4.1.2. Base

The block diagram of the base of the mechanism is shown in "Fig. 7", which was imported from the SolidWorks software. This block diagram, as can be seen, includes the framework, definition of the reference coordinate system and gravitational acceleration direction, the solver characteristics, the coordinate axes defining the base position, and the connections to the sliders.
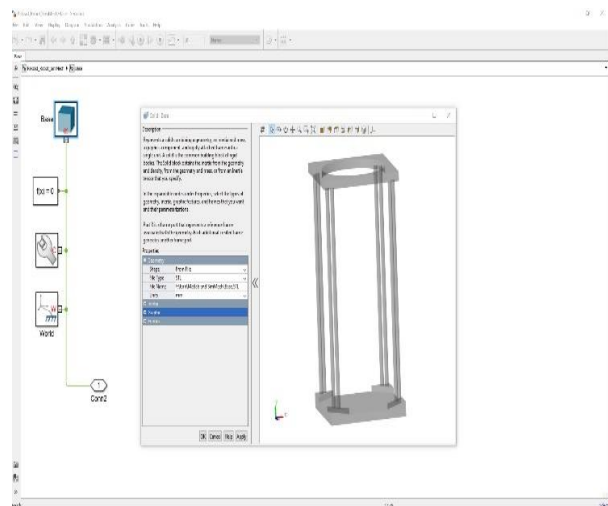
Fig. 7   The base block of the Simmechanic model of the studied mechanism.

4.1.3. Sliders

The slider block diagram for the example is shown in "Fig. 8". This block diagram contains the framework, joints, coordinate axes, and inputs of the movement and the force output conditions. The input signals from the input block diagram (analytical method) have to be converted to sliders with a specific unit using the Simulink signal converter to the physical input signal. The default units are according to the SI system (m, kg and s).
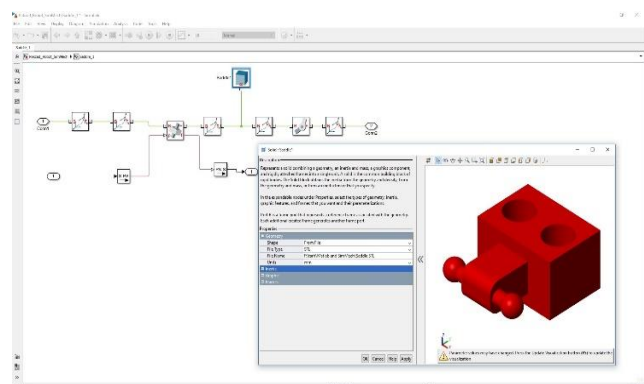
Fig. 8   The slider block of the Simmechanic model of the studied mechanism.

4.1.4. Links

In the mechanism studied, each pods of the mechanism consists of two links, as shown in "Fig. 5", as well as that is clear; two links connected to the sliders. The block diagrams of link 1,1 for the example is shown in "Fig. 9". This block diagram also includes the framework, the joints, the coordinate axes connected to the slider on one side and the moving platform to the other.
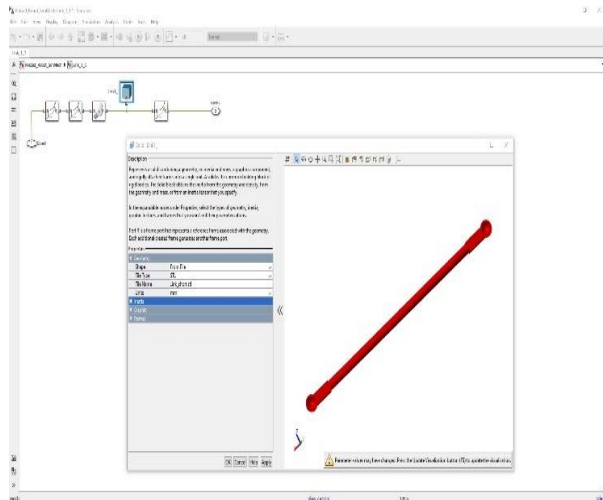
Fig. 9 The link block of the Simmechanic model of the studied mechanism.

4.1.5. Moving Platform

As shown in "Fig. 10", the moving platform is connected to the four pods, the pods 1 and 3 being connected by the connector and the pods 2 and 4 directly connected to the moving platform as shown in the block diagram containing the framework, joints, and coordinate axes.
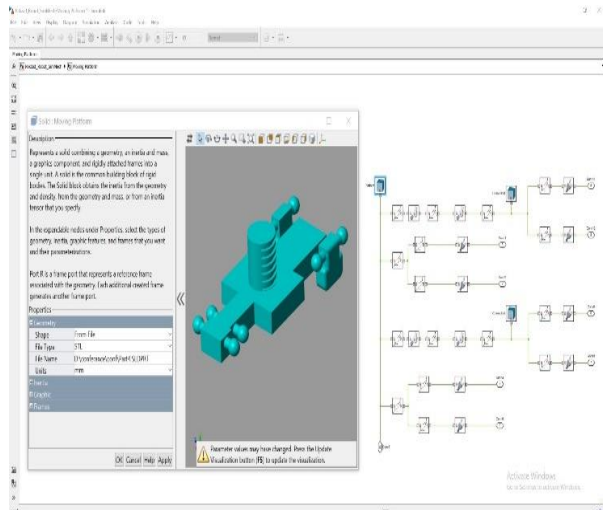
Fig. 10 The moving platform block of the Simmechanic model of the studied mechanism.

4.1.6. Driving forces output

The forces obtained from the sliders are collected and shown in the Scope block in accordance with "Fig. 11".
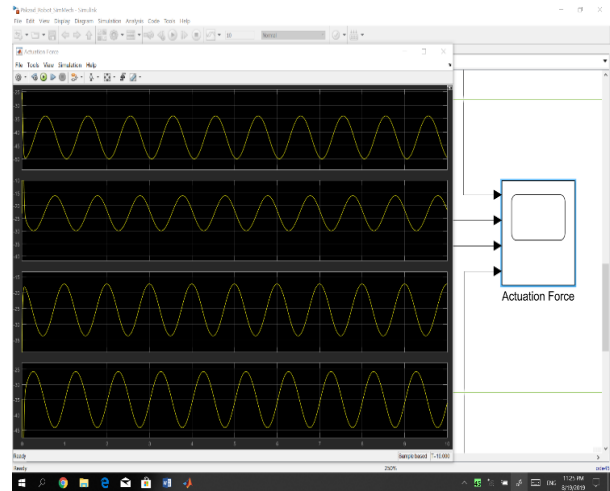
Fig. 11 The output block of the Simmechanic model of the studied mechanism.

4.2. Validation Results of Inverse Dynamics Analysis by Theory and Simulation Method

To validate, the proposed 3D printer will print a cylinder in 10 seconds with the specifications of "Table 1". To print the specified geometry, the 3D printer nozzle must follow a circular path according to "Fig. 12". For this motion of nozzle, the four drives of the printer must traverse the specific motions that are determined using the inverse position Kinematics, velocity and acceleration are also shown in "Fig. 13".

Table 1 Geometry of print specifications

Radius of the cylinder	50 mm
Height of the cylinder	10 mm
Used nozzle	0.5 mm
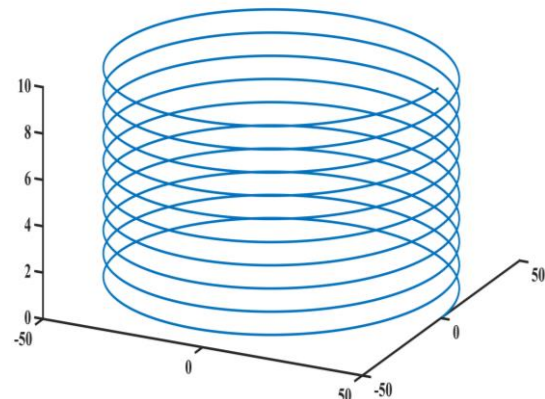
Fig. 12 The nozzle path for validating the inverse dynamics model.
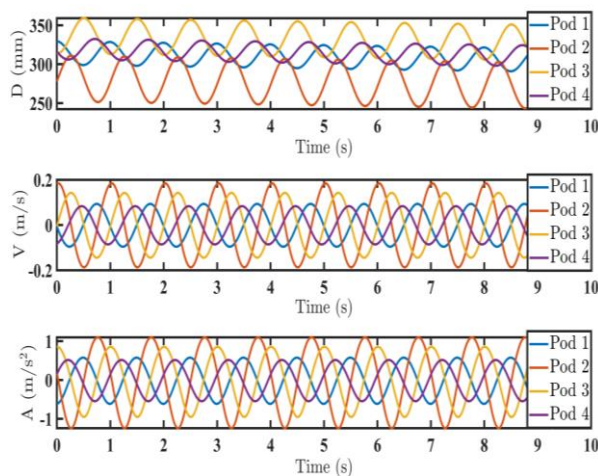
Fig. 13   Position, velocity and acceleration of slider pods based on nozzle motion for print of table 1 geometry in 10 seconds.

The calculated forces using the analytical equations and the Simmechanic model for the specified path are shown in "Fig. 14". It is observed that the results of the proposed model and the Simmechanic model are approximately equal indicating the accuracy of the proposed dynamic model.
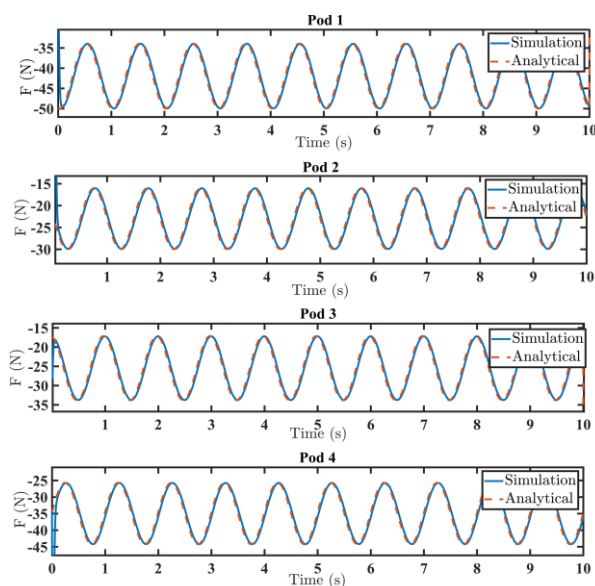
Fig. 14   Comparison of calculated forces using analytical relationships and Simmechanic model of slider based on nozzle motion for print of Table 1 geometry in 10 seconds.

5   INFLUENCE OF PRINT SPEED ON MOTION AND DRIVERS FORCES

Obviously, if the printer nozzle travels the designated path in less time, the drives must move with more velocity and more acceleration. Figures 15-17 show the

comparison of drives motions if the printer nozzle follows the specified path in 5, 10, 20, and 40 seconds, respectively based on position, velocity, and acceleration. In the case of the position diagram as shown, the drives anyway follow the path shown on the rails, although their navigation time varies. In velocity and acceleration graphs, it is also evident that at faster nozzle movements, the velocity and acceleration of the drives also increase and are directly related to the nozzle speed.
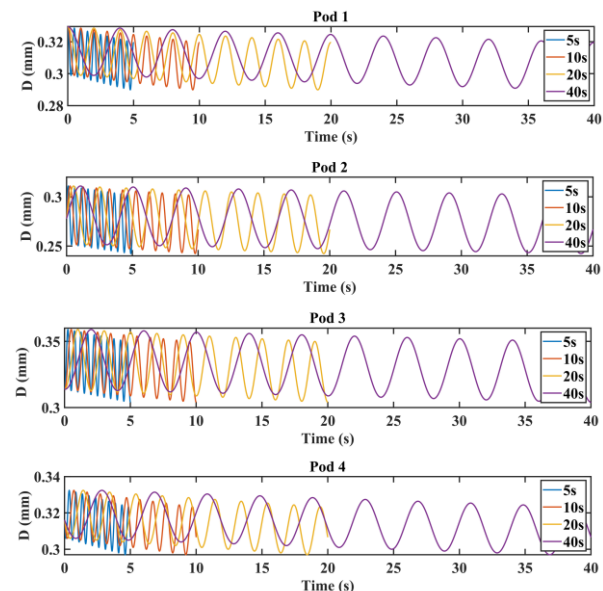
Fig. 15   Comparison of printer drives position based on nozzle motion for Table 1 geometry printing at 5, 10, 20 and 40 seconds.
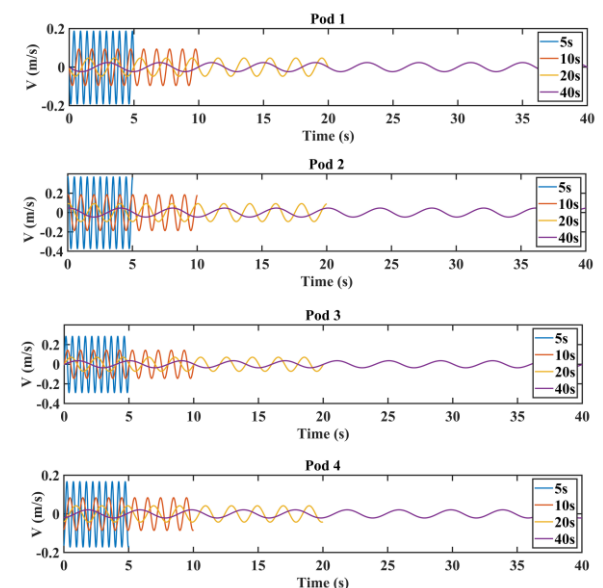
Fig. 16   Comparison of printer drives velocity based on nozzle motion for Table 1 geometry printing at 5, 10, 20 and 40 seconds.
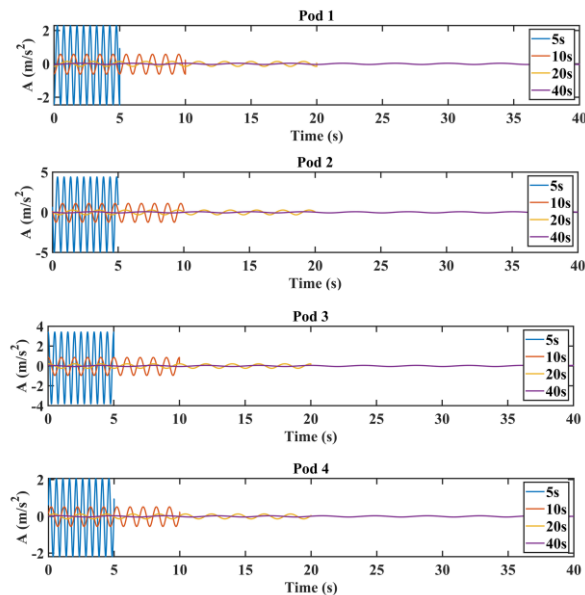
Fig. 17   Comparison of printer drives acceleration based on nozzle motion for Table 1 geometry printing at 5, 10, 20 and 40 seconds.

The purpose of this analysis is to investigate the effect of nozzle speed on the force required to entered drives to provide the nozzle motion. The effect of nozzle movement on the velocity and acceleration of the drives was observed, which is also evident. However, the effect of this movement on the force drives is shown in "Fig. 18". At 10, 20, and 40-second motions, the force entered drives is approximately the same, but at 5-second motions, the drives forces have grown impressively.
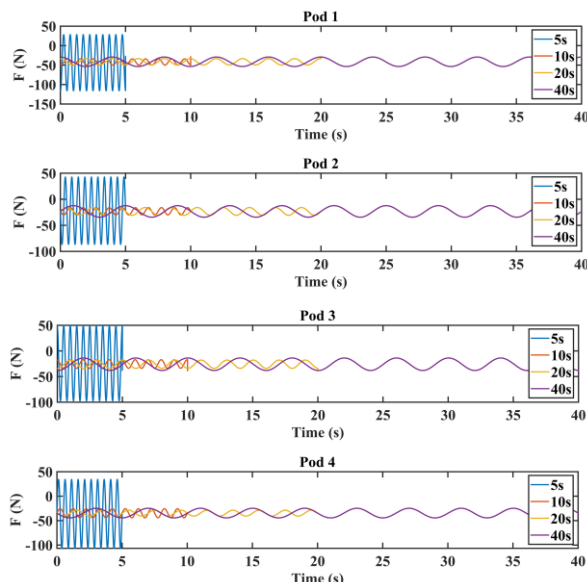
Fig. 18   Comparison of printer drives force based on nozzle motion for Table 1 geometry printing at 5, 10, 20 and 40 seconds.

6   CONCLUSION

With regard to the "Eq. (15)" driving forces, it consists of several parameters including inertia, Coriolis and friction which are observed among the parameters. So that as long as the contribution of Coriolis force to the other forces is low, the effects of changes in velocity and acceleration on total force is too low but when the velocity and acceleration increase, and of course due to its high power in relation to the total force, the Coriolis force contribution also increases and its effect can be seen as shown in "Fig. 18" in a very fast 5-second motion. Therefore, it is advisable to traverse the nozzle at times exceeding 10 seconds to avoid wasting energy and reducing depreciation. Since the limits of forces are the same at times of more than 10 seconds, therefore the best time to time saving is 10 seconds in the specified path. Due to the velocity and acceleration of the drives in 10 seconds, it is better to use this range in defining other paths to print.

REFERENCES

[1]   Tsai, L. W., Robot Analysis: The Mechanics of Serial and Parallel Manipulators, Wiley, 1999.

[2]   Wu, J., Yin, Z., A Novel 4-DOF Parallel Manipulator H4 in Parallel Manipulators, Towards New Applications, Huapeng Wu, I-Tech Education and Publishing, 2008, pp. 405–448.

[3]   Stewart, D., A Platform with Six Degrees of Freedom, Proceedings of the Institution of Mechanical Engineers, Vol. 180, 1965, pp. 371–386.

[4]   Merlet, J. P., Parallel Robots. Springer, 2006.

[5]   Geng, Z., Haynes, L. S., Lee, J. D., and Carroll, R. L., On the Dynamic Model and Kinematic Analysis of a Class of Stewart Platforms, Robotics and Autonomous Systems, Vol. 9, No. 4, 1992, pp. 237–254.

[6]   Lebret, G., Liu, K., and Lewis, F. L., Dynamic Analysis and Control of a Stewart Platform Manipulator, Journal of Robotic Systems, Vol. 10, No. 3, 1993, pp. 629–655.

[7]   Pang, H., Shahinpoor, M., Inverse Dynamics of a Parallel Manipulator, Journal of Robotic Systems, Vol. 11, No. 8, 1994, pp. 693–702.

[8]   Caccavale, F., Siciliano, B., and Villani, L., The Tricept Robot: Dynamics and Impedance Control, IEEE/ASME Transactions on Mechatronics, Vol. 8, No. 2, 2003, pp. 263–268.

[9]   Abdellatif, H., Heimann, B., Computational Efficient Inverse Dynamics of 6-DOF Fully Parallel Manipulators by Using the Lagrangian Formalism, Mechanism and Machine Theory, Vol. 44, No. 1, 2009, pp. 192–207.

[10] Do, W. Q. D., Yang, D. C., Inverse Dynamic Analysis and Simulation of a Platform Type of Robot, Journal of Robotic Systems, Vol. 5, No. 3, 1988, pp. 209–227.

[11] Reboulet, C., Berthomieu, T., Dynamic Models of a Six Degree of Freedom Parallel Manipulators, Fifth International Conference on Advanced Robotics 'Robots in Unstructured Environments, Pisa, Italy, 1991.

[12] Ji, Z., Study of the Effect of Leg Inertia in Stewart Platforms, Proceedings IEEE International Conference on Robotics and Automation, Atlanta, GA, USA, 1993.

[13] Harib, K. H., Dynamic Modeling, Identification and Control of Stewart Platform-Based Machine Tools, the Ohio State University, Columbus, Ohio, 1997.

[14] Dasgupta, B., Mruthyunjaya, T. S., A Newton-Euler Formulation for The Inverse Dynamics of the Stewart Platform Manipulator, Mechanism and Machine Theory, Vol. 33, No. 8, 1998, pp. 1135–1152.

[15] Dasgupta, B., Mruthyunjaya, T. S., Closed-Form Dynamic Equations of the General Stewart Platform through the Newton–Euler Approach, Mechanism and Machine Theory, Vol. 33, No. 7, 1998, pp. 993–1012.

[16] Dasgupta, B., Mruthyunjaya, T. S., Erratum to 'Closed-Form Dynamic Equations of the General Stewart Platform through the Newton — Euler Approach' [Mechanism and Machine Theory 33 (7) 993–1012], Mechanism and Machine Theory, Vol. 35, No. 4, 2000, p. III.

[17] Riebe, S., Ulbrich, H., Modelling and Online Computation of the Dynamics of a Parallel Kinematic with Six Degrees-Of-Freedom, Archive of Applied Mechanics, Vol. 72, No. 11-12, 2003, pp. 817–829.

[18] Guo, H. B., Li, H. R., Dynamic Analysis and Simulation of a Six Degree of Freedom Stewart Platform Manipulator, Proceedings of The Institution of Mechanical Engineers Part C-journal of Mechanical Engineering Science, Vol. 220, 2006, pp. 61–72.

[19] Khalil, W., Ibrahim, O., General Solution for The Dynamic Modeling of Parallel Robots, Journal of Intelligent and Robotic Systems, Vol. 49, No. 1, 2007, pp. 19–37.

[20] Wang, J., Wu, J., Wang, L., and Li, T., Simplified Strategy of the Dynamic Model of A 6-UPS Parallel Kinematic Machine for Real-Time Control, Mechanism and Machine Theory, Vol. 42, No. 9, 2007, pp. 1119–1140.

[21] Mahmoodi, A., Menhaj, M. B., and Sabzehparvar, M., An Efficient Method for Solution of Inverse Dynamics of Stewart Platform, Aircraft Engineering and Aerospace Technology, Vol. 81, No. 5, 2009, pp. 398–406.

[22] Clavel, R., Conception d'un Robot Parallèle Rapide À 4 Degrés De Liberté, Lausanne, EPFL, Thesis, 1991.

[23] Wang, J., Gosselin, C. M., A New Aproach for the Dynamic Analysis of Parallel Manipulators, Multibody System Dynamics, Vol. 2, No. 3, 1998, pp. 317–334.

[24] Gallardo, J., Rico, J. M., Frisoli, A., Checcacci, D., and Bergamasco, M., Dynamics of Parallel Manipulators by Means of Screw Theory, Mechanism and Machine Theory, Vol. 38, No. 11, 2003, pp. 1113–1131.

[25] Tsai, L. W., Solving the Inverse Dynamics of a Stewart-Gough Manipulator by the Principle of Virtual Work, Journal of Mechanical Design, Vol. 122, No. 1, 2000, pp. 3.

[26] Nguyen, C. C., Pooran, F. J., Dynamic Analysis of A 6 dof Ckcm Robot End-Effector for Dual-Arm Telerobot Systems, Robotics and Autonomous Systems, Vol. 5, No. 4, 1989, pp. 377–394.

[27] Fujimoto, K.; Kinoshita, Y.; Maeda, K.; Tadokoro, S., and Takamori, T., Derivation and Analysis of Equations of Motion for 6-DOF Direct-Drive Wrist Joint, Proceedings IROS '91: IEEE/RSJ International Workshop on Intelligent Robots and Systems '91, Osaka, Japan, 1991, pp. 2–7.

[28] Miller, K., Clavel, R., The Lagrange-Based Model of Delta-4 Robot Dynamics, Robotersysteme, No. 8, 1992, pp. 49–54.

[29] Liu, K., Lewis, F., Lebret, G., and Taylor, D., The Singularities and Dynamics of a Stewart Platform Manipulator, Journal of Intelligent and Robotic Systems, Vol. 8, No. 3, 1993, pp. 287–308.

[30] Miller, K., Optimal Design and Modeling of Spatial Parallel Manipulators, The International Journal of Robotics Research, Vol. 23, No. 2, 2004, pp. 127–140.

[31] Kebria, P., Abazari, M. R., and Abdi, H., Simmechanics Model Development for Gantry-Tau Robot.

[32] Craig, J. J., Introduction to Robotics: Mechanics and Control, Pearson Prentice Hall, Upper Saddle River, Vol. 3, 2005.